NURETH14-568

ALGEBRAIC TURBULENT HEAT FLUX MODEL FOR PREDICTION OF THERMAL STRATIFICATION IN PIPING SYSTEM

M. Pellegrini¹, H. Endo², E. Merzari³, H. Ninokata¹,

Nuclear Engineering Department, Tokyo Institute of Technology, Japan
 Japan Nuclear Energy and Safety Organization (JNES), Tokyo, Japan
 Nuclear Engineering Division, Argonne National Laboratory (ANL), Argonne, IL, USA

Abstract

The effect of stratification on the flow in bounded geometries is studied through computational fluid dynamics (CFD) and two different modeling of the turbulent heat flux, namely constant turbulent Prandtl number and Algebraic Heat Flux Model (AHFM). The main feature of the work is the evaluation of the effect of buoyancy on the thermal quantities, velocity field and related pressure drop. It has been stated the superiority of the AHFM for the evaluation of turbulent heat flux and temperature field together with a correct evaluation of the thickness of the thermal layer (i.e stratification persistence), in comparison with the simple eddy diffusivity approach. However the adopted model shows over-prediction of the momentum transport in the vertical direction in comparison with the experimental data introducing higher uncertainties for the obtained pressure drop and related Fanning friction factor.

Introduction

The evaluation of the interactions between fluids moving with different densities has interested researchers belonging to various fields: from two-phase and two-fluids to stratified flows resulting from distribution of concentration and temperature in a gravitational field. Stratification was at the beginning studied for natural phenomena such as lakes, oceans and estuaries [1], where currents of different velocity and density introduce processes which are partially unknown. The study of wide liquid basins can be approximated with free shear layers, meaning that the flow is not bounded and wall effects can be neglected. Through this assumption still the study maintains a high order of reliability and physical understanding of the process.

Recently the same problem was posed in engineering fields inside piping systems [2] and [3], in scenarios where thermal transients, introduced in accident conditions, creates drastic flow reduction and high temperature variations. A thermal ramp at the pipe inlet creates a non equilibrium interface driving the hotter flow in the vertical direction and generating two layers of different density and velocity. This issue in previous works was addressed mainly because of the creation of radial temperature distribution on the pipe walls inserting thermal stresses on the structure, which could lead to loss of structure integrity. To the best of the authors' knowledge

however, the analysis of the pressure drop and the modification on the Fanning friction factor due to stratification were not deeply investigated and this represents the main motivation moving the research of the present paper in this direction.

In the work provided in [4] large eddy simulation (LES) was employed for the analysis of various different regimes of stratified flows in channel geometry; the same author focuses on the employment of open channel so that higher Reynolds numbers can be computed saving computational efforts. This approach, as hinted above, concentrate on the mixing layer region and how gravity might influence the turbulent and vertical transport in it, nevertheless the effect of the walls are of secondary importance.

In case of completely bounded flows analysis, as in the case of our interest, the employment of LES would ask a high computational effort which would result in extremely long time for the computation. Indeed the employment of turbulence modeling (Reynolds stresses and turbulent heat flux) and near wall treatment modeling, still represent powerful tools in order to assess the major characteristics of the flow and investigation of various conditions (different Reynolds and Richardson numbers) to possibly find correlations to be implemented in "coarser" codes (e.g. system codes). Nevertheless, stratification regime in pipes introduces a real challenge for modeling due to coexistence of various flow regimes, density and temperature variation, and buoyancy effect.

It was demonstrated how the simple assumption of turbulent eddy diffusivity does introduce many uncertainties and wrong predictions in stratified flows [5]. Various methodologies therefore could be employed for a better estimation of turbulence suppression due to gravity; in the work provided by [6] the suppression of turbulent transport in the vertical direction was addressed through the contribution of additional damping functions on the Reynolds stresses and turbulent heat flux. While the work in [6] shows quite important insights about stratification mechanisms, the introduction of damping functions appear not general in case different fluids or geometry are to be employed. In the present work the authors therefore aim to evaluate the validity and generality of an Algebraic Heat Transfer Model (AHFM) in application to thermally stratified flows in bounded geometries. Essential validations are indeed needed for a model which might be widely employed in the future in nuclear applications in relation to buoyancy driven flows.

1. Shear stresses

Pressure drop arising in bounded flows depends on the stresses introduced inside the system. In homogenous flows in pipes, stresses are created because of the non-slip condition applied to the flow by the wall. Evaluation of losses was held by various scientists which, thanks to diverse investigations, suggested correlations for laminar and turbulent flows [7].

In stratified flows in addition, shear stresses are introduced because of velocity difference in the bulk of the flow creating a mixing layer. The analysis of isothermal free plane mixing layer was held by many scientists and formalized by Pope [8]. It was observed that the mixing layer in an open space, grows linearly and has a preferential direction towards the slow moving front.

Considering two parallel flows discharging in an open space with two different velocities U_t and U_b ($U_t < U_b$) it is possible to characterize the flow through some relevant parameters:

$$U_{c} = \frac{1}{2} (U_{t} + U_{b})$$

$$U_{s} = U_{b} - U_{t} \qquad ,$$

$$\langle U(x, y_{\alpha}(x), 0) \rangle = U_{t} + \alpha (U_{b} - U_{t})$$

$$(1)$$

where α assumes values from 0 to 1. In this way it is possible to define the thickness of the mixing layer as:

$${}^{1}\delta(x) = y_{0.9}(x) - y_{0.1}(x). \tag{2}$$

It has to be noticed that in stratified flows the above two phenomena appear simultaneously, while their behavior seems completely different and almost opposite. Indeed, while a mixing layer grows expanding towards the walls, the boundary layer develops towards the center of the pipe. It appears clear that eventually the constrains imposed by the walls will uniform the flow and it will behave as homogenous moving in a pipe with average velocity U_c. The question we want to address in the present paper is therefore contrary to the general issue addressed in pipe geometries and in particular: how long the flow configuration will be far from the one imposed by the walls and to which extent buoyancy will affect on its persistence during the thermal transient?

For the evaluation therefore the focus of the study is on the developing region, the region where boundary and mixing layer grow and on the assessment to the degree which gravity will sustain the developing region both dynamically and thermally.

2. Experiment: Geometry and Discretization

The simulation refers to the experimental data provided by [9] whose geometry is shown in Figure 1.

In the settling chamber the flow is divided into two streams by a splitter plate which, at the end, forms a knife for preventing flow separation. Both flows pass through a nozzle and create the uniform velocity and temperature distributions which characterize the flow at the pipe inlet. The non dimensional numbers which drive the flow are the bulk Reynolds number $Re_b = \frac{U_c D}{V_c}$ and the

bulk Richardson number $Ri_b = \frac{g\beta\Delta TD}{U_s^2}$. The values of velocity, temperature, non dimensional numbers and geometry adopted for the present simulation, are provided in Table 1.

¹ Values 0.9 and 0.1 are completely arbitrary.

The 14^{th} International Topical Meeting on Nuclear Reactor Thermalhydraulics, NURETH-14 Toronto, Ontario, Canada, September 25-30, 2011

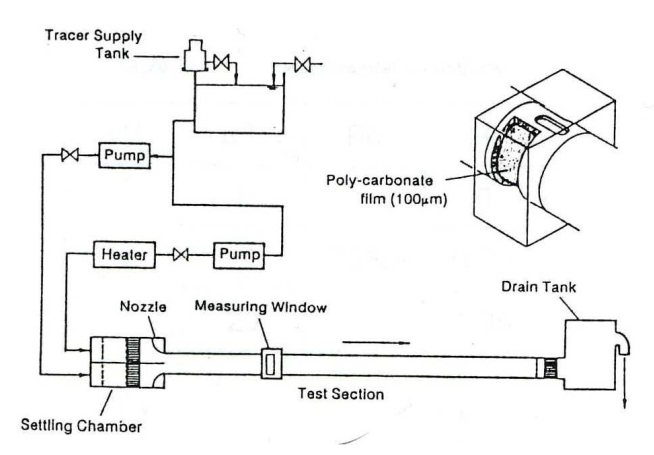


Figure 1 Experimental apparatus [9].

Table 1 Parameters governing the benchmark.

U_t [m/s]	U_b [m/s]	T _t [K]	T _b [K]	ΔT [K]	Ri	Re	D [m]
0.106	0.146	291.15	311.15	20	1.36	7350	0.06

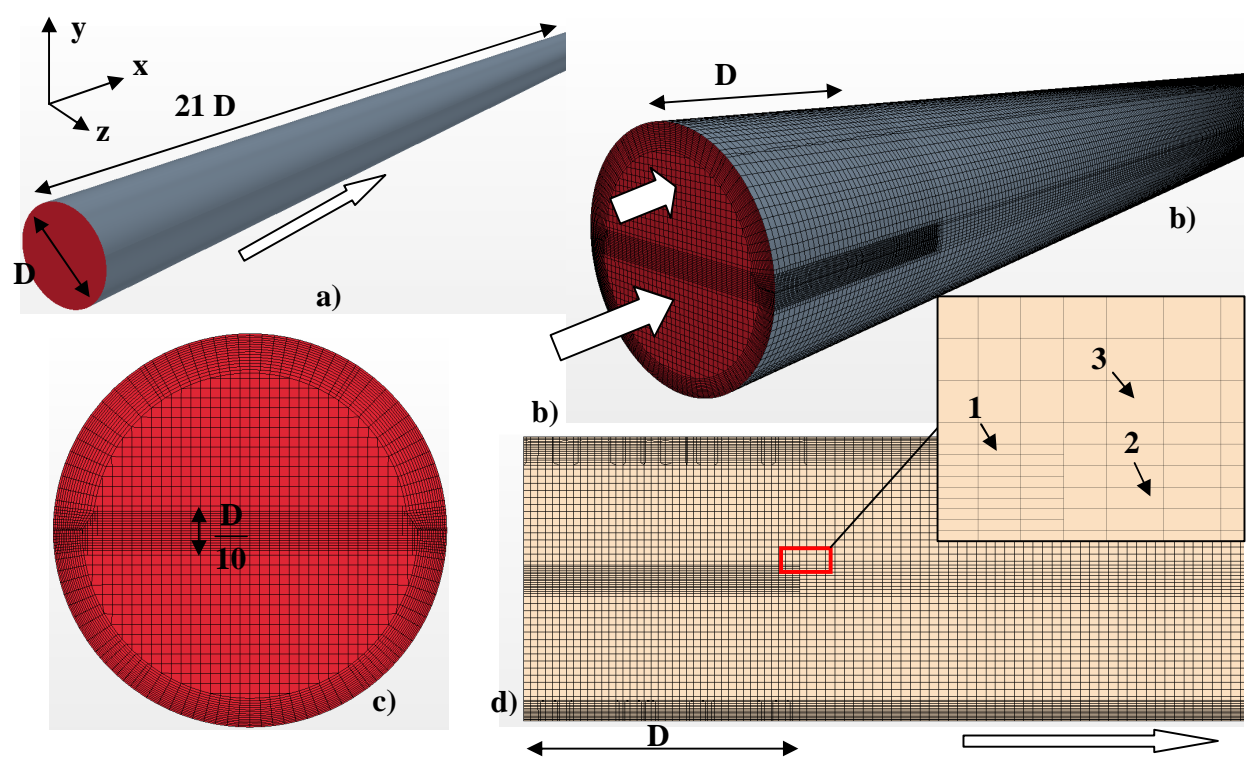


Figure 2 Discretized geometry. a) pipe dimensions; b) total discretization; c) particular of the discretization on the inlet, d) particular of the symmetry plane. White arrows represent the flow direction. Highlighted points' measures are: 1) 0.375 mm; 2) 0.75 mm; 3) 1.5 mm.

The discretization adopted in the simulation is shown in Figure 2. Prism layer was created on the wall so to obtain the proper y^+ (y^+ < 1 in the first cell from the wall). Due to the different local Reynolds number of the upper and lower streams, boundary layers have different thickness (Figure 2c).

Shear layer introduces high velocity gradients which must be computed and discretized with a finer grid in the center of the domain; for this reason a volume shape refinement [10] was created in the center of the domain with a finer discretization close to the inlet (1D from the inlet as shown in Figure 2 b and d) and thickness equal to D/10 (Figure 2c). Values of characteristic mesh size are identified in the blow up of Figure 2 d and described in the caption; 1) refers to the minimum size in the bulk in order to discretize the high gradient region at the inlet, 2) refers to the size of the shear layer discretization in the rest of the domain, which presents milder gradients, 3) is the largest cell size adopted in the domain. The final mesh resulted to have less than 1,900,000 hexaedrical cells. The mesh independency was evaluated through the building of a finer mesh which results in the computation of similar flow characteristics (velocity, temperature). The spatial discretization shown in Figure 2 was therefore employed in the calculations.

3. CFD Methodology

The computational code employed in the present work is the commercial code STAR-CCM+6.02.007 [10]. The equations shown in this chapter and in the appendix will be solved in second-order accuracy in space. Convective terms are discretized with second order upwind scheme. The flow is solved as incompressible and the connection between continuity and momentum equations is achieved with Rhie-Chow pressure-velocity coupling combined with the SIMPLE algorithm. The density is assumed constant during the calculations and expression of the buoyancy force in the momentum equation follows the Boussinesq approximation (truncation to the first order of the Taylor expansion). The RANS equations which are employed in the analysis are:

$$\frac{\partial U_j}{\partial x_j} = 0 \tag{3}$$

$$\frac{DU_{j}}{Dt} = -\frac{1}{\rho} \frac{\partial P}{\partial x_{j}} + \frac{\partial}{\partial x_{i}} \left(v \frac{\partial U_{j}}{\partial x_{i}} - \overline{u_{i}} \overline{u_{j}} \right) + g \beta (T - T_{0}) \delta_{i2}$$
(4)

$$\frac{DT}{Dt} = \frac{\partial}{\partial x_i} \left(\frac{\kappa}{c_p \rho} \frac{\partial T}{\partial x_i} - \overline{\theta u_i} \right),\tag{5}$$

where the terms $\overline{u_iu_j}$ and $\overline{\theta u_i}$ need a closure. The closure of the first term (i.e. Reynolds stresses) was performed through standard k- ε low Reynolds model [11]. The choice of a linear model was done for two main reasons, it was found that it provides reliable results in the isothermal case (Chapter 4.1) and it increases the stability of the AHFM reaching a more than acceptable level of convergence also in steady state simulations for all the quantities. However, as shown by [12], standard k- ε model is likely to introduce anomaly in case of high shear stress which, in case of the employment of AHFM, resulted in upset of the simulation. This problem can be solved through the introduction of scale limiter which guarantees the realizability. Even though this issue would deserve a more detailed attention, nevertheless in the present paper a proper discussion is not included because beyond the scope of the analysis, anyhow further analyses in this direction might be done in the future.

The closure of the second term (turbulent heat flux) is performed through two different models which will be compared in the paper and defined as AHFM and constant Pr_t or simple gradient diffusion hypothesis (SGDH) in the rest of the paper. For the latter the assumption of constant eddy diffusivity was employed which can be succinctly described as:

$$\overline{\theta u_i} = -\alpha_t \frac{\partial T}{\partial x_i} = -\frac{v_t}{\Pr_t} \frac{\partial T}{\partial x_i}$$
(6)

where Pr_t is the turbulent Prandtl number which was set equal to 0.9. For the former modeling instead the present paper refers to the work provided by [13] and its formalization is given in appendix.

Regarding the boundary conditions, two different velocities (see Table 1) are applied at the inlet with a constant distribution and covering the upper and lower half of the boundary respectively. Finally walls in the domain are considered adiabatic and with no-slip conditions.

4. Results

Results are provided at three locations of the geometry and respectively at x/D = 4; 8; 12.

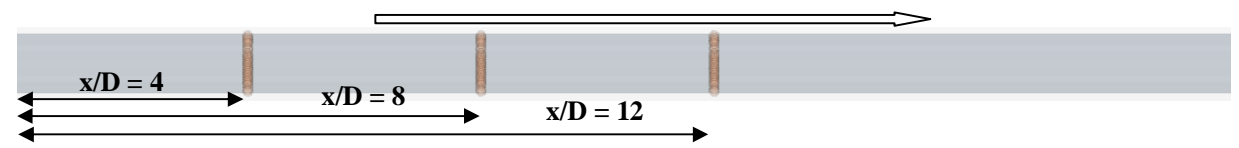


Figure 3 Location of the monitoring lines for the flow evaluation. White arrow represents the flow direction.

4.1. Isothermal flow results

The present case represents a straight pipe which is one of the most studied flow regimes in CFD applications and modeling, however the presence of two different and flat velocity profiles applied as inlet conditions, leads to the creation of various regimes (i.e. boundary layers development, mixing layer with shear stress) in a relatively small domain. This results in a not

obvious analysis and indeed also the isothermal flow represents a hard task for a proper CFD modeling. This is because damping functions are generally developed and studied for completely developed flows and considerations of equilibrium between turbulence production and dissipation might not be valid in a domain where the highest turbulent energy production is in the bulk of the domain rather than closer to the wall.

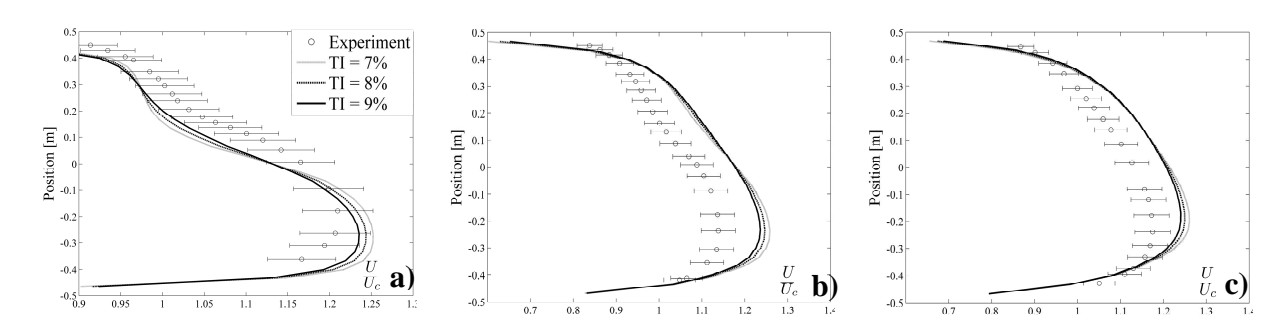


Figure 4 Isothermal results. Three cases with different turbulence intensity (TI) were tested as a sensitivity analysis.

Sensitivity analysis for the isothermal case was done to assess the turbulence intensity, after several tests a value of 9% was found to be the one which provides better agreement. This value is typical for turbulence after a grid as in the performed experiment. Figure 4 shows that a perfect agreement cannot be obtained, even though the shape of velocity and the characteristics of the mixing layer (creation of inflection points) are generally described. Large deviations in the bulk are to be attributed to the near wall evaluation. The boundary layer indeed appears to grow faster in the simulation than in the experiment leading to create wide zones of grater velocities. Nevertheless, due to formulation of the damping functions, which allow all the equations to be solve all the way to the wall, in comparison to other common approaches (e.g. two-layer and standard wall functions) this appears to be the most general way to approach the problem.

The different boundary layer growth is thought to affect also the correct prediction of pressure drop, which was introduced as one of the objects of the analysis, nevertheless more important for our aim is the evaluation of how buoyancy can influence on the mixing layer persistence and how it will affect the total pressure drop.

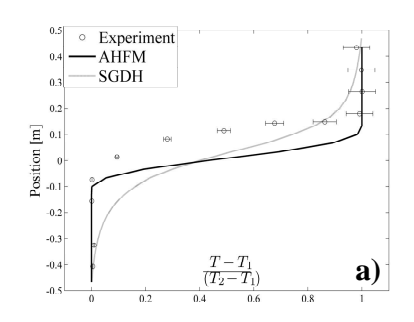
4.2. Non isothermal flow results

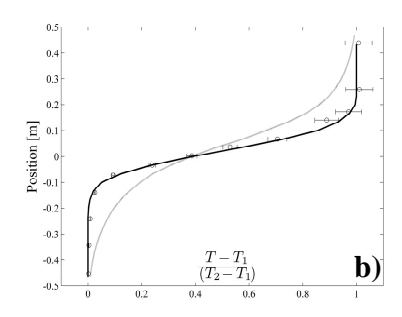
In this chapter results achieved with two models for the turbulent heat flux will be compared. As a reminder the two cases will be referred to as *AHFM* and *SGDH*.

4.2.1. <u>Temperature profiles and mixing layer thickness</u>

The evaluation of the temperature (Figure 5) as expected shows that the employment of constant Pr_t overestimates the heat transferred between the two layers and the erosion of the thermal

mixing layer appears much quicker compared to the prediction of the AHFM and the experimental data. This behavior results from the definition of the turbulent heat flux that, as shown in equation (6) directly connects the heat transferred because of turbulence (i.e. turbulent heat flux) to the temperature gradient only. The AHFM on the other side shows much more accurate prediction of the temperature field along the pipe, in particular for the thickness of the stratification (e.g. the slope) in the thermal mixing layer for all the locations. Nevertheless it should be noticed that in Figure 5 a) the disagreement of AHFM is about the location of temperature gradient. This behavior might be a consequences of wake creation at the interface close to the inlet where the flow could show instabilities in the mixing layer, driving the location of the mixing layer in a non symmetrical location across the centerline. However this behavior is not predicted in the flow, which can be solved via steady calculation for all the variables.





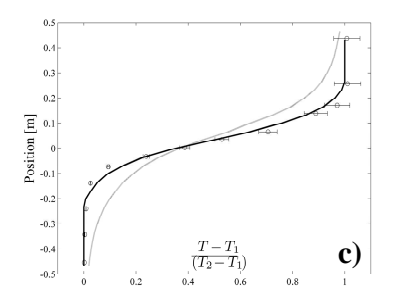


Figure 5 Temperature profiles.

The analysis of the thermal mixing layer thickness is shown in Figure 6. In the experimental paper [9] the thickness was evaluated as the 25% difference between the temperature average. Referring to equation it can be easily written assuming $\alpha = 0.25$ and 0.75. Prediction of the AHFM demonstrates that the absolute value of the temperature width is reasonably accurate. The constant Prandtl number model shows absolute values of the thermal thickness far from the one assessed experimentally but with a similar trend (constant values at the end of the pipe).

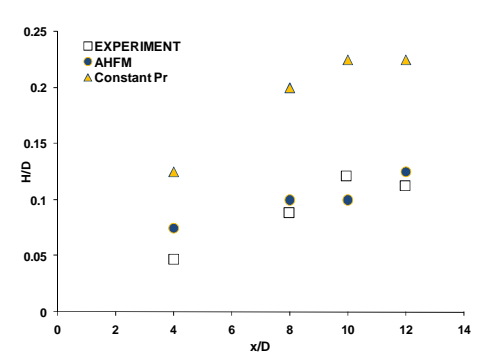


Figure 6 Thermal mixing layer thickness

This aspect can be explained referring to Figure 5. Since further in the domain temperature gradient becomes less steep, in the same extent also the molecular and turbulent heat flux predicted by the SGDH decreases and thermal thickness does not greatly increase from two consecutives locations.

4.2.2. <u>Turbulent heat fluxes</u>

In Figure 7 turbulent heat flux was compared at the three locations. The AHFM data show an excellent agreement in the first two locations, the agreement is judged in relation to the peak values and the width in the y-direction. Constant Pr-t model instead shows very poor predictions (one order of magnitude difference in the first two locations) which is responsible for the high heat transferred in the y-direction.

Figure 7 c) needs instead a special explanation. In the experiment the authors evaluates the creation of a counter-gradient heat flux (positive turbulent heat flux) at 12 diameters from the inlet. This phenomenon is the one responsible for the decreasing in the thermal mixing layer thickness found at location x/D = 12 in Figure 6, phenomenon which cannot be replicated by the present simulation for both AHFM and SGDH. This phenomenon is the result of the interaction of turbulent heat transfer and Reynolds stresses, in this extend therefore a higher order modeling for $\overline{u_i u_j}$ should be considered. However, as explained above, this leads the present simulation to be less stable and, in the present analysis, only a linear model is employed. In this direction therefore a more complete analysis should be done.

This is responsible for the increase of the thermal mixing layer thickness, resulting in slightly not precise predictions of the thermal field far from the domain inlet (Figure 5c).

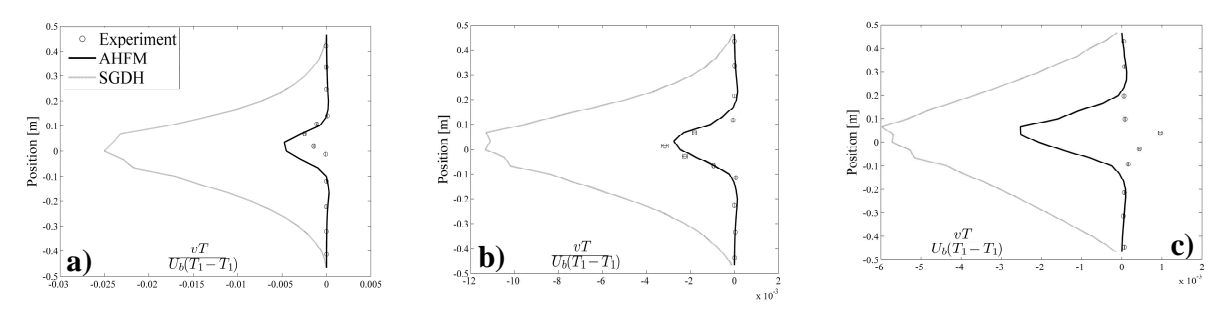


Figure 7 Turbulent heat flux comparison.

4.2.3. Velocity profile and pressure drop

Figure 8 a), b) and c) show the comparison against experimental data of stratification effect on velocity. While in the isothermal case the achieved results are basically inside the measurement error of the experiment, velocity profiles for the non-isothermal case differ quite consistently from the available data. The main effect is assessed against Figure 4, indeed both models delay the creation of the uniform velocity profile respect to the isothermal case, inflection points are

visible at location x/D = 8. Based on the knowledge gained for the isothermal flow, modeling of the Reynolds stresses and wall is found to greatly affect the velocity field and therefore unlikely that, even though well performance of the AHFM, velocity field could provide better agreement than what achieved for the isothermal one. Through the employment of constant turbulent Prandtl number the velocity profile is also affected; this should not be surprising since the wide extent of the thermal mixing layer for the present model. More correct instead the behavior of AHFM that, even though characterized by a thinner thermal layer, shows similar effect on velocity.

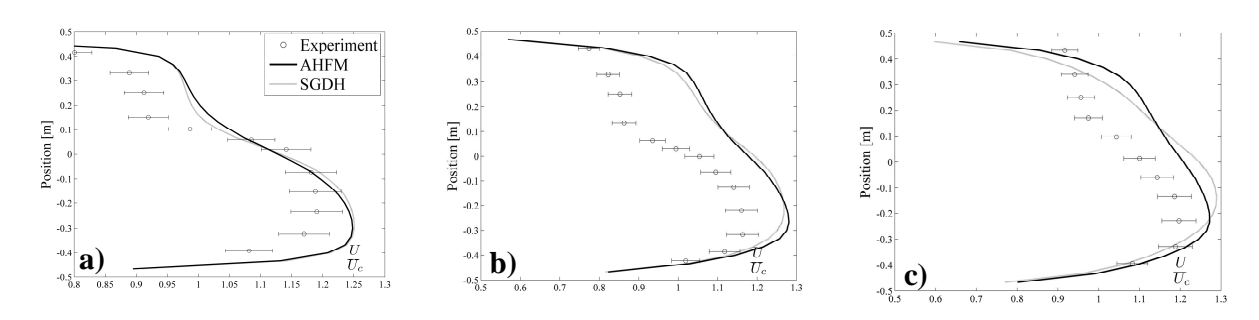


Figure 8 a) through c) velocity comparison at the three locations. d) represents the vectorial representation of the mixing layer erosion predicted by AHFM in the three locations.

Figure 9 shows an effect on pressure drop due to buoyancy compared to isothermal flows. There is basically no difference between the pressure drop predicted by the two thermal models since, as shown above, velocity profiles are indeed similar. What should be highlighted is that the insertion of temperature has the effect of decreasing turbulence which in the end affects also the pressure drop. The isothermal case shows a Fanning friction factor in agreement with the value obtained at Reynolds number defined on U_c due to high values of turbulence intensity, while lower friction factors are obtained for nonisothermal cases. Nevertheless in relevant engineering cases, the isothermal flow with mixing layer is not likely to occur or anyhow not relevant for this evaluation.

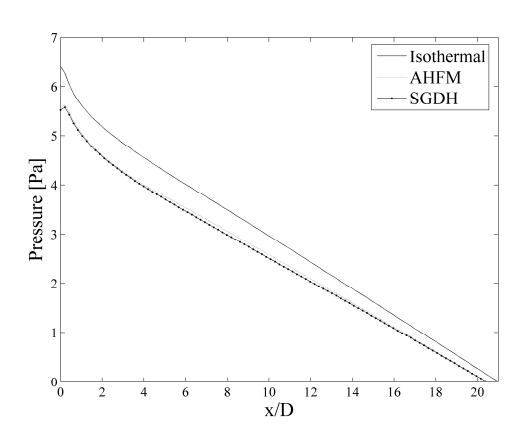


Figure 9 Pressure drop along the x-direction.

The insertion of thermal transient at low Reynolds number are the setting conditions in order to create shear and mixing layer and affecting the pressure drop inside the piping system and during the transient.

The evaluation of the pressure drop indicates that, if the developing regions would last longer, as predicted in the experimental case, this would introduce a consistent modification of the friction factor which would have an important role in the natural circulation flow evaluation. This motivation and the surprising result achieved above are the reasons for a further investigation which should be performed in this direction.

5. Conclusions

We have performed a simulation of thermally stratified turbulent flow in a straight pipe through two different models for the turbulent heat flux. The employment of AHFM shows that high agreement is obtained for the temperature field and turbulent heat flux, however the effect that buoyancy has on the velocity field appears to be underestimated and the momentum transport in the vertical direction shows disagreement with the experimental data. The AHFM was generally employed for the evaluation of natural convection experiment (Rayleigh-Bernard cells, eccentric annulus) and the focus was hold principally on the thermal part (Nusselt number assessment); in this case however, since we focus on the thermal effect of gravity on the flow, the interactions between the two fields introduce additional uncertainties of the modeling, which is stated by the higher disagreement of the velocity fields. Even though the results seem satisfactory for the temperature, which is also of primary importance for the prediction of thermal stresses on the structure, the present work cast doubts which will need further investigation.

APPENDIX - ALGEBRAIC HEAT FLUX MODEL (AHFM)

The AHFM is obtained by the truncation of the parent model differential transport equations for $\overline{\theta u_i}$ where the reduced expression assuming production and dissipation of k and $\overline{\theta}^2$ are locally in balance. The general algebraic expression can be written as:

$$\overline{\theta u_i} = -C^{\theta u} \frac{k}{\varepsilon} \left(C_0^{\theta u} \overline{u_i u_j} \frac{\partial T}{\partial x_j} + C_1^{\theta u} \overline{\theta u_j} \frac{\partial U_i}{\partial x_j} + C_2^{\theta u} \beta g \overline{\theta^2} \right). \tag{7}$$

Equation (7), even though simplified, contains the three major contributor from the transport equation of the turbulent heat flux, the non-uniformity of the thermal field (∇T), the mean rate of strain (∇U_i) and the attenuation or amplification of turbulence due to the effect of buoyancy $\beta g \overline{\theta^2}$. It should be noted that neglecting the effect of mean strain of rate and buoyancy leads the definition of $\overline{\theta u_i}$ to the so called generalized gradient diffusion hypothesis, where the turbulent heat flux still depends basically on the gradient of temperature but the component of the

Reynolds stresses still influence its value. In case the Reynolds stress tensor its replaced with its trace the formulation of equation (7) collapses into (6) or simple gradient diffusion hypothesis (SGDH).

The closure of the algebraic expression requires that the four scalar introduced: k, ε , $\overline{\theta}^2$, ε_θ be provided from additional transport equations, therefore finally our model will need to solve a four equation model $k - \varepsilon - \overline{\theta}^2 - \varepsilon_\theta$. The equation are shown hereafter, also the transport equation for k and ε , which contain different gravity contribution respect to the terms presented in case of SGDH, will be shown:

$$\frac{Dk}{Dt} = D_k + P_k + P_g - \varepsilon \tag{8}$$

$$\frac{D\varepsilon}{Dt} = D_{\varepsilon} + \frac{\varepsilon}{k} \left(C_{\varepsilon 1} P_k + P' + C_{\varepsilon 3} P_g + P_{nl} \right) - C_{\varepsilon 2} f_2 \rho \left(\varepsilon - \varepsilon_0 \right)$$
(9)

$$\frac{D\overline{\theta^2}}{Dt} = D_k + 2P_\theta - 2\varepsilon_\theta \tag{10}$$

$$\frac{D\varepsilon_{\theta}}{Dt} = D_{\varepsilon\theta} + \frac{\varepsilon_{\theta}}{\overline{\theta^2}} \left(C_{\varepsilon 1}^{\theta} P_{\theta} + C_{\varepsilon 2}^{\theta} P_{\theta} \frac{\varepsilon}{\varepsilon_{\theta}} \frac{\overline{\theta^2}}{k} + C_{\varepsilon 3}^{\theta} P_{k} \frac{\overline{\theta^2}}{k} + C_{\varepsilon 4}^{\theta} \varepsilon_{\theta} - C_{\varepsilon 5}^{\theta} \varepsilon \frac{\overline{\theta^2}}{k} \right)$$
(11)

where:

$$P_{k} = -\overline{u_{i}u_{j}} \frac{\partial U_{i}}{\partial x_{j}}, \quad P_{g} = -\beta g_{i} \overline{\partial u_{i}}, \quad P_{\theta} = -\overline{\theta u_{i}} \frac{\partial T}{\partial x_{j}}$$

$$P' = f_{2} \left(P_{k} + 2\mu \frac{k}{y^{2}} \right) \exp\left(-0.00375 \operatorname{Re}_{y}^{2} \right)$$

$$D_{\varphi} = \frac{\partial}{\partial x_{j}} \left[\left(\nu + C_{\varphi} f_{\mu} \frac{k^{2}}{\varepsilon} \right) \frac{\partial \varphi}{\partial x_{j}} \right]$$

$$f_{\mu} = 1 - \exp\left[-\left(C_{d0} \sqrt{\operatorname{Re}_{y}} + C_{d1} \operatorname{Re}_{y} + C_{d2} \operatorname{Re}^{2} \right) \right], \quad f_{2} = 1 - 0.3 \exp\left(\operatorname{Re}_{T}^{2} \right)^{2}, \quad (12)$$

and the index φ for D_{φ} , eq. (12), stands for any variables which is solved by the related transport equation.

Besides the standard coefficients employed for k and ε equations ($C_k = 0.09$, $C_{\varepsilon} = 0.07$, $C_{\varepsilon 1} = C_{\varepsilon 3} = 1.44$, $C_{\varepsilon 2} = 1.92$). the additional coefficients are specified in Table 2.

 $^{^{2}}$ P_{nl} , which can be easily found in [10] is not shown in the appendix due to its formulation which is not the central aim of the work.

Table 2 Adopted coefficients.

$C_0^{ heta u}$	$C_1^{ heta u}$	$C_2^{ heta u}$	$C_3^{\theta u}$	$C^{ heta}_{arepsilon 1}$	$C^{ heta}_{arepsilon 2}$	$C^{ heta}_{arepsilon 3}$	$C^{ heta}_{arepsilon 4}$	$C^{ heta}_{arepsilon 5}$	$\sigma_{_{ heta 2}}$	$\sigma_{arepsilon heta}$
0.2	0.6	0.6	0.3	1.3	0.0	0.72	2.2	0.8	1.0	1.3

Acknowledgment

The authors would like to acknowledge the THINS project for providing the present study with the suitable tools in order to perform simulations with the AHFM and the support received during the analysis.

References

- [1] E. J. Hopfinger. "Turbulence in stratified fluids: a review", Journal of Geophysical Research, Vol. 92, No. C5, 1987, pp. 5287-5303.
- [2] K.E. Kasza, J.P Bobis, W.P. Lawrence, "Overview of thermal transient induced buoyancy phenomena in pipe and heat exchanger flows", Chemical Engineering Communication, Vol. 19, 1983, pp. 295-316.
- [3] Y. Ashurko, G. Pugachev, "Phenomenon of coolant local natural circulation occurring in heat removal loops of nuclear power plant", Journal of Nuclear Science and Technology, Vol. 48, No. 4, 2011, pp. 602-611.
- [4] P. Garg, J. H. Ferziger, S. G. Monismith, J. R. Koseff, "Stably stratified turbulent channel flows. I. Stratification regimes and turbulence suppression mechanism", Physics of Fluids, Vol. 12, No. 10, 2000, pp. 2569-2594.
- [5] G. Grötzbach, "Anisotropy and buoyancy in nuclear turbulent heat transfer critical assessment and needs for modeling", Forchungszentrum Karlsruhe, Wissenschaftliche Brichte, FZKA 7363, December 2007.
- [6] S. Murakami, S. Kato, T. Chikamoto, D. Laurece, D. Blay, "New low-Reynolds-number k-ε model including damping effect due to buoyancy in a stratified flow field", International Journal of Heat and Mass Transfer, Vol. 39, No. 16, 1996, pp. 3483-3496.
- [7] R. B. Bird, W. E. Stewart, E. N. Lightfoot, "Transport phenomena: Second Edition", John & Wiley, 2007.
- [8] S. B. Pope, "Turbulent flows", Cambridge University Press, 2000.
- [9] K. Kobayashi, K. Ishida, M. Maeda, "Turbulent transport across stable thermal stratified layer in a circular pipe", <u>Proceeding 9th International Heat Transfer Conference</u>, Jerusalem, Israel, Vol. 5, pp 341-346, 1990.
- [10] STAR-CCM+6.02 User's Guide.
- [11] F.S. Lien, W.L. Chen, M.A. Leschziner, "Low-Reynolds number eddy-viscosity modelling based on non-linear stress-strain/vorticity relations", <u>Proc. 3rd Symp. on Engineering Turbulence Modelling and Measurements</u>, Crete, Greece, 27-29 May, 1996.

- [12] P.A. Durbin, "On the k-3 stagnation point anomaly", International Journal of Heat and Fluid Flow, Vol. 17, 1996, pp. 89-90.
- [13] K. Hanjalic, "One-point closure models for buoyancy-driven turbulent flows", Annual Review Fluid Mechanics, Vol. 34, 2002, pp. 321-347.
- [14] M. Pellegrini, H. Endo, H. Ninokata, "Numerical investigation of bent pipe flows at transitional Reynolds number", Progress in Nuclear Energy, 2011, doi:10.1016/j.pnucene.2011.02.005.